View Letter

Close

Date: 23-06-2016
To: "Claudio L. A. Berli" cberli@santafe-conicet.gov.ar
cc: j.c.t.eijkel@utw ente.nl
From: "Jan Eijkel" j.c.t.eijkel@utw ente.nl
Subject: MANO: Your manuscript entitled A quantitative model for lateral flow assays

---

Ref.: Ms. No. MANO-D-16-00116R1
A quantitative model for lateral flow assays
Microfluidics and Nanofluidics

Dear Dr. Berli,

I am pleased to inform you that your w ork has now been accepted for publication in Microfluidics and Nanofluidics.

Thank you for submitting your w ork to this journal.

With kind regards

Jan Eijkel, Ph.D.
Editor-in-Chief
Microfluidics and Nanofluidics

—

****

Close

Microfluid Nanofluid manuscript No.
(will be inserted by the editor)

A quantitative model for lateral flow assays

Claudio L. A. Berli · Pablo A. Kler

Received: date / Accepted: date

Abstract A simple mathematical model that quantitatively describes the dynamics of analyte capture in lateral flow assays is presented. The formulation accounts for the capillary-driven flow through the porous membrane, the advective transport of analyte, and the immunoreactions that takes place in the detection line. Model predictions match the numerical results obtained by computer simulations of the full advection-diffusion-reaction problem in the operating regime of lateral flow assays. The main system parameters were condensed into two dimensionless numbers, namely the relative fluid velocity and the relative analyte concentration. The system is then completely characterized in the space of these critical numbers. The model is also able to describe the time evolution of analyte binding by using alternative time scalings, which discriminate different experimental conditions. The equations reported are practical tools for the design and optimization lateral flow tests, enabling informed decisions on basic questions such as the appropriate flow rate, sample volume, or assay time. Beyond lateral flow assays, the work offers an improved understanding of the underlying physico-chemical processes involved in paper-based microfluidics.

1 Introduction

Lateral flow assays are well established tests for rapid and easy detection of a large variety of biological and chemical markers (Wong and Tse, 2009). As the technique satisfies all the requirements to be implemented in resource-limited settings, mainly for public health in developing countries (Yager et al, 2006), the development of test strips is experiencing a renaissance on these days, which is also motivated by the high research activity in paper-based microfluidics (Mace and Deraney, 2014; Yetisen et al, 2013; Cate et al, 2015).

Improving the existing technologies requires, among other things, the introduction of quantitative determinations and enhanced detection limits. These challenges demand large experimental efforts,

Claudio L. A. Berli
Instituto de Desarrollo Tecnológico para la Industria Química (INTEC, UNL–CONICET)
Colectora RN 168 Km 472. S3000GLN Santa Fe, Argentina. E-mail: cberli@santafe-conicet.gov.ar

Pablo A. Kler
Centro de Investigación de Métodos Computacionales (CIMEC, UNL–CONICET)
Colectora RN 168 Km 472. S3000GLN Santa Fe, Argentina.E-mail: kler@cimec.santafe-conicet.gov.ar

because the optimization of novel materials and reaction schemes is currently made empirically. In fact, despite the large experience gained in the field, quantitative descriptions of how assay parameters influence the analyte capture efficiency are not available in the scientific literature. Straightforward questions (but of significant practical relevance) such as the appropriate concentration of capture sites or the optimal fluid velocity are usually solved via experimentation. In this context mathematical models able to explore different assay conditions would be of practical interest to lateral flow test developers, as well as for microfluidic researchers.

Comprehensive theoretical models for surface binding in microfluidic systems are available (Hu et al, 2005; Gervais and Jensen, 2006; Parsa et al, 2008; Squires et al, 2008; Hansen et al, 2012; Aguirre et al, 2014), which involve the coupling of advective transport, molecular diffusion, and chemical reactions. These formulations are very useful to understand the physicochemical basis of the general problems, however the practical implementation invariably requires numerical computations. For the specific case of lateral flow assays, theoretical calculations are barely found in the literature. A mathematical model of strip test was reported for sandwich (Qian and Bau, 2003) and competitive assays (Qian and Bau, 2004). The formulation includes a complete set of immunoreactions and computations were made on commercial simulation tools. However practical information is not easily extracted from numerical results and critical parameters are not identified. More recently, a mathematical model to predict the optimal test line location (x_L in Fig. 1) and sample volume was reported (Ragavendar and Anmol, 2012). Another numerical approach (Zeng et al, 2012) makes use of particle filtering techniques to estimate the state of different assay parameters from experimental data of the detection line. Numerical calculations were also used to explore different membrane shapes (Mendez et al, 2009), assay architectures (Parolo et al, 2013), and fluidic delays (Choi et al, 2016). The last three works simulated the flow through the membranes without computing immunoreactions.

The present work proposes a mathematical model that describes the dynamics of the analyte capture process in lateral flow assays. In contrast to the above mentioned approaches, which demand numerical computations and require experts analysis, here a simple analytical model is reported. It is based on algebraic expressions of ease computation, and explicitly includes the key system parameters, namely the relative flow rate and the relative analyte concentration. Thus the model serves as a handy tool for the design and optimization of lateral flow tests. The next section describes the problem formulation, the hypothesis made, and the analytical solution in terms of critical system parameters. Afterwards the numerical calculation of the full transport-diffusion- reaction problem is presented, which was implemented to validate the predictions of the analytical model. Finally we discuss the capability of the proposed model to quantitatively describe the essential features of lateral flow test.

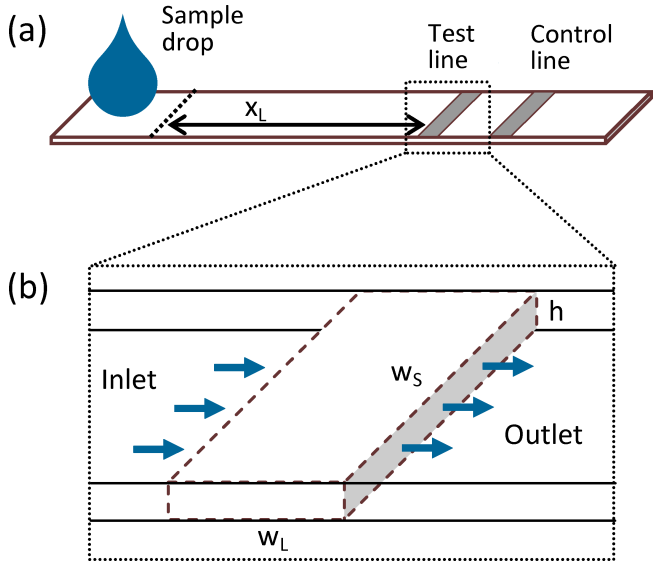

Fig. 1: (a) Schematic representation of the basic test strip, where x_L measures the location of the test line. (b) Geometry of the reaction zone considered to model the analyte transport and capture: the dashed lines define a volumetric reaction zone, where w_L is the test line width, w_s is the strip width (test line length), and h is the membrane thickness.

2 Theoretical modeling

2.1 Problem statement

Initially we define the flow domain and the kinetic problem to be modeled, which also involves immunoreactions. The assay takes place on a paper-like strip, typically nitrocellulose, with the geometry sketched in Fig. 1a. The test begins when a drop of sample is laid over one of the strip ends. The sample is an aqueous solution containing the analyte, which has been previously incubated with a label agent. Capillary action drives the fluid towards the opposed strip end, where a capture line is located to specifically bind the analyte. Analyte capture occurs while the sample flows through the reaction zone (Fig. 1b); the accumulation of captured analyte (conjugated to the label agent) produces a visible signal on the test line. The flow continues until capillary action is interrupted due to sample volume limitation, or because the fluid front reaches the strip end. A control line is also included in the membrane, which is prepared to specifically bind the label agent.

The reaction volume $V_L = w_L w_s h$ is the membrane volume associated to the capture zone, comprised by the test line width (w_L) and the cross-sectional area ($w_s h$) traversed by the fluid flow (Fig. 1b). The rate of analyte capture, $r = -dC_A/dt$, follows the standard immune-reaction kinetics

$$r = k_b C_A C_S - k_u C_{AS} \tag{1}$$

where C_A, C_S, and C_{AS} are, respectively, the concentrations of analyte (either antigen or antibody), capture site (the inmuno counterpart of the analyte) and reaction product (antigen- antibody complex). In addition k_b and k_u are the binding and unbinding constants, respectively, the ratio of which constitutes the equilibrium constant $K = k_b/k_u$.

For the capture sites inmmobilized in the reaction zone, the initial concentration fixed to the membrane must satisfy, $C_S^0 = C_S + C_{AS}$. As a first approximation, here we consider that capture sites are uniformly distributed in the considered domain, and species concentrations are average values in the volume V_L. On the other hand, the analyte is unidirectionally transported by the flow, hence describing the dynamics of C_A requires additional considerations, as discussed below.

2.2 Dynamics of capillary imbibition

Capillary imbibitions in paper-like substrates has been well described in the recent literature (Masoodi and Pillai, 2010; Wang et al, 2013; Shou and Fan, 2015; Elizalde et al, 2015). The flow is assumed to be stationary and free of inertia, because of the very low Reynolds numbers reached at the pore level. For homogeneous strips, at isothermal conditions and with controlled humidity level, the average velocity of the fluid front reduces to

$$u(x) = c/x \tag{2}$$

where $c = \kappa \Delta p/(\mu\phi)$ is a coefficient that characterizes the whole system: Δp is Laplace's pressure due to capillarity, ϕ is the medium porosity, μ is the fluid viscosity and κ the permeability of the porous substrate. For water in nitrocellulose, $c \approx 1-10$ mm^2/s, depending on the membrane microstructure. Time integration of Eq. 2 leads to the typical $x \sim t^{1/2}$ imbibition kinematics.

According to Eq. 2, the sample reaches the capture zone at the velocity $u_L = c/x_L$, considering $t = 0$ when the fluid is at the starting position (dotted line in Fig. 1). Thus the analyte flux can be adjusted by varying the location of the detection line (distance x_L), which is known to have a significant impact on assay sensitivity. Nevertheless, as changing x_L also influences both the amount of sample required and the assay time, other strategies to control the fluid front velocity are being explored as well (Jahanshahi-Anbuhi et al, 2012; Shin et al, 2014; Elizalde et al, 2015; Choi et al, 2016).

2.3 Characteristic times

The analyte is transported by the flow, and while passing through the reaction zone, molecules diffuse toward the capture sites and react to form the complex. The relative importance of each process can be studied from the respective time scales:

– The residence time of the analyte in the capture zone is $t_r = w_L/u_L$, considering that fluid velocity does not change appreciably across the test line ($w_L \ll x_L$; Fig. 1). Introducing the volumetric flow rate $Q = u_L w_S h$, the residence time also represents the time required to exchange one reaction volume, $t_r = V_L/Q$. In practice, $x_L \approx 20$mm and $w_L \approx 1$mm, thus $t_r \approx 20$s.

- The diffusive time is $t_D = d^2/D$, where D is the molecular diffusion coefficient ($\approx 10^{-10}\mathrm{m}^2/\mathrm{s}$, IgG in nitrocellulose, (Moghadam et al, 2015) and d is the membrane pore diameter ($\approx 10\mu\mathrm{m}$). Therefore $t_D \approx 1\mathrm{s}$.
- The characteristic kinetic time can be estimated as $t_k = (k_b C_A^0)^{-1}$ from the forward term of the reaction equation. For typical immunoassays, $k_b \approx 10^4(\mathrm{Ms})^{-1}$ and $C_A^0 \approx 100\mathrm{nM}$, thus $t_k \approx 10^3\mathrm{s}$.

It is readily seen that analyte diffusion is much faster than chemical reaction, hence analyte capture occurs in the so-called reaction-limited condition(Kockmann, 2008), in other words, the complex formation is the limiting step of the analyte capture process. Under these conditions, the capture dynamics is characterized by the balance between the residence and reaction times (Gervais and Jensen, 2006). This scaling analysis agrees with the practical knowledge in the field: controlling the sample flow rate is critical to optimize the capture efficiency. Therefore, here we introduce the relative fluid velocity:

$$U = \frac{c}{x_L w_L k_b C_s^0} = \frac{Q}{V_L k_b C_s^0} \tag{3}$$

as a critical system parameter. The second equality in Eq. 3 represents the relative flow rate, which can be also interpreted as the advective transport rate divided by the characteristic reaction rate. In addition, U coincides with the reciprocal of the first Damköhler number used in microprocess engineering (Gervais and Jensen, 2006; Kockmann, 2008).

2.4 Transport model for the analyte

Given the situation of chemical control, a macroscopic balance of the analyte moles in the reaction volume is expressed (Kockmann, 2008),

$$QC_A|_{inlet} - QC_A|_{outlet} \approx rV_L \tag{4}$$

where QC_A accounts for the moles per unit time entering/leaving the reaction zone with the flow (Fig. 1b). A pseudo steady state is assumed, where the analyte flux through the reaction volume (left hand side of Eq. 4) equals the rate of consumption by the immunoreaction. Fluid velocity is c/x_L at the inlet and $c/(x_L + w_L)$ at the outlet. For $w_L \ll x_L$, Eq. 4 is rewritten as,

$$\frac{u_L}{w_L}(C_A^0 - C_A) \approx k_b C_A (C_S^0 - C_{AS}) - k_u C_{AS} \tag{5}$$

where C_A^0 is the analyte concentration entering the reaction zone. This flux balance leads to an explicit expression of the analyte concentration in terms of fluid velocity,

$$C_A = \frac{k_u C_{AS} + C_A^0 \frac{u_L}{w_L}}{k_b (C_S^0 - C_{AS}) + \frac{u_L}{w_L}} \tag{6}$$

where C_A and C_{AS} are instantaneous (time dependent) values. In particular, at the very early stages of the reaction, $C_{AS} \approx 0$ and $C_A/C_A^0 \approx U/(1+U)$. This relationship predicts that the analyte concentration exiting the reaction volume increases with flow rate. Thus the formulation grasps the trend expected in practice: the capture efficiency improves when fluid velocity decreases.

2.5 Kinetic model for the complex formation

Taking into account that the rate of antigen-antibody complex formation is equivalent to the rate of analyte capture, $r = dC_{AS}/dt = -dC_A/dt$, the complex concentration C_{AS} is governed by Eq. 1, where the analyte concentration C_A can be substituted by the pseudo steady state solution obtained above (Eq. 6). The following non-linear differential equation is obtained for $C_{AS}(t)$:

$$\frac{dC_{AS}}{dt} = k_b\Big[\frac{k_u C_{AS} + C_A^0 \frac{u_L}{w_L}}{k_b(C_S^0 - C_{AS}) + \frac{u_L}{w_L}}\Big](C_S^0 - C_{AS}) - k_u C_{AS} \tag{7}$$

Defining the dimensionless variables $\overline{C}_{AS} = C_{AS}/C_S^0$ (relative complex concentration) and $\bar{t}_k = t/t_k$ (relative kinetic time), and reordering the terms, Eq. 7 is rewritten as follows:

$$\frac{d\overline{C}_{AS}}{d\bar{t}_k} = \frac{1 - \overline{C}_{AS}(1 + 1/KC_A^0)}{1 + (1 - \overline{C}_{AS})U^{-1}} \tag{8}$$

this governing equation involves two critical system parameters: the relative fluid velocity U and the normalized initial analyte concentration KC_A^0.

In the limiting case of $U \to \infty$, Eq. 8 becomes a linear equation, the solution of which is the Langmuir-type adsorption kinetics ($Da \to 0$),

$$\overline{C}_{AS} = \overline{C}_{AS}^{\infty}(1 - e^{-(\overline{C}_{AS}^{\infty}\ \bar{t}_k)}) \tag{9}$$

with the initial condition $\overline{C}_{AS} = 0$, $\bar{t}_k = 0$. In this solution, $\overline{C}_{AS}^{\infty} = KC_A^0/(1+KC_A^0)$ is the maximum occupation of capture sites ($\bar{t}_k \to \infty$). Equation 9 has been recently used to discuss the detection limits of lateral flow assays (Moghadam et al, 2015), however it is valid for constant analyte concentration only (negligible capture). Here, Eq. 9 is useful to illustrate the influence of KC_A^0 . For instance, if $KC_A^0 = 1$, then, $\overline{C}_{AS}^{\infty} = 1/2$, meaning that only 50% of capture sites will be occupied at equilibrium, due to the balance between binding and unbinding processes. Besides, KC_A^0 serves as metric of the detection limits in immunoassays, the best values reached in practice are $KC_A^0 \approx 10^{-2}$ (Moghadam et al, 2015). Furthermore, for such low KC_A^0 values, one observes that the amount of complex formed is directly proportional to the initial analyte concentration, a fact of practical interest in the design of quantitative analysis.

For arbitrary U values, Eq. 8 still admits analytical solution, though in the implicit form $\bar{t}_k(\overline{C}_{AS})$. In fact, integrating with the initial condition $\overline{C}_{AS} = 0$, $\bar{t}_k = 0$, yields,

$$\overline{t_k} = \frac{\overline{C}_{AS}U^{-1} - [1 + (1 + KC_A^0)^{-1}U^{-1}]\ln[1 - (1 + 1/KC_A^0)\overline{C}_{AS}]}{1 + 1/KC_A^0} \tag{10}$$

It should be mentioned that a solution analogous to Eq. 10 has been reported (Hansen et al, 2012) for pseudo steady state operation of open flow-cells with surface reactions. Precisely, the kinetic time scale $\bar{t}_k$ is more suitable for systems without sample volume limitations. Considering the characteristics of test strips, where sample volume is limited, here we introduce the relative flow time, $\bar{t}_r = t/t_r$. As t_k and t_r are related by U, Eq. 10 is easily rewritten in the form $\bar{t}_r(\overline{C}_{AS})$:

$$\overline{t_r} = \frac{\overline{C}_{AS} - [U + (1 + KC_A^0)^{-1}]\ln[1 - (1 + 1/KC_A^0)\overline{C}_{AS}]}{(1 + KC_A^0)/KC_S^0} \tag{11}$$

Both Eqs. 10 and 11 represent the time evolution of complex formation, or equivalently the fraction of bound sites, for the same physical problem, though with different time scaling. In particular, the relative flow time also represents the relative reacted sample volume, that is $\bar{t}_r = V_S(t)/V_L$, where $V_S(t)$ is the sample volume that pass through the reaction zone at time t. Finally, Eq. 11 is reordered to solve for U vs $\overline{C}_{AS}$ as follows,

$$U = \frac{\overline{C}_{AS} - (V_S/V_L)(1 + KC_A^0)/KC_S^0}{ln[1 - (1 + 1/KC_A^0)\overline{C}_{AS}]} - \frac{1}{1 + KC_A^0} \tag{12}$$

This expression allows one to investigate the dynamics of complex formation as a function of flow rate, in the space of the dimensionless numbers KC_A^0 , KC_S^0 , and V_S/V_L , which are the main design parameters of lateral flow assays.

3 Numerical Simulation

In order to develop an internal validation of the practical model, numerical simulation were performed using a Finite Element Method (FEM) tool. Besides the 3D calculation domain, in this case the differences between the practical model and the simulations were: (i) the existence of a finite diffusion coefficient D_A for the analyte; (ii) finite lengths before and after the test line; and finally, (iii) continuous variation of the velocity according to Eq. 2.

3.1 Software

Numerical simulations were performed with a previously developed FEM tool using the program PETSc-FEM as the numerical calculation platform in a Python environment. This simulation tool was already validated for several analytical applications (Kler et al, 2011, 2013). The simulations were performed on a desktop computer with single quad-core Intel i7 3770 3.4 GHz processor, 16

GB DDR3-1066 memory, using 4 calculation threads. Data postprocessing was performed with Paraview(Ayachit, 2015), NumPy, SciPy and Matplotlib (van der Walt et al, 2011).

3.2 Simulation conditions

The geometry of the calculations domain for the FEM calculations were $x_L = 20$ mm,$w_s = 5$ mm,$h = 10$ μm, and $w_L = 1$ mm. In order to perform the analysis for different values of t_r, the total length of the modeled strip was $l = 30$mm. FEM mesh consisted of 15000 hexahedrons distributed as a structured uniform mesh. Initial concentrations for analyte and capture sites were $C_A^0 = C_S^0 = 100$ nM, diffusion coefficient for the analyte was $D_A = 10^{-12}\mathrm{m^2s^{-1}}$. Finally, the values of k_b, k_u and c were varied in order to match the different values for U proposed by the analytical model: 10^4 $(\mathrm{Ms})^{-1} \leq \mathrm{k_b} \leq 6.4\ 10^5$ $(\mathrm{Ms})^{-1}$, 10^{-3} $\mathrm{s^{-1}} \leq \mathrm{k_u} \leq 6.4\ 10^{-2}$ $\mathrm{s^{-1}}$, $1.3\ 10^{-6}\mathrm{m^2s^{-1}} \leq \mathrm{c} \leq 7.8125\ 10^{-8}\mathrm{m^2s^{-1}}$. Initial velocity was chosen in order to develop a suitable initial condition for solving Eq. 14, i.e.:

$$||\mathbf{u}_L||_{t=0} = \frac{c}{\mathrm{CFL\ h_{FEM}}} \tag{13}$$

3.3 Simulation scheme

The simulation procedure involves the iterative coupling of analytical calculations for the fluid velocity and front position, and the numerical simulation of transport and reaction processes. After initial conditions for the fluid velocity and concentrations, the first step consists in setting an adequate timestep (Δt) for the FEM simulation. In order to determine this value, we use the following equation:

$$\Delta t = \min\left\{\frac{\mathrm{CFL\ h_{FEM}}}{||\mathbf{u}_L||}\right\} \tag{14}$$

where CFL accounts for the Courant-Friedrich-Levy condition (Donea and Huerta, 2003) that we define with an optimum value of 0.95, and $h_{FEM} = 10\mu$m is the finite element mesh parameter, which results from dividing the domain length by the total number of mesh elements. Once the timestep is determined, one solving iteration of the transport–reaction equation is performed by using the velocity field previously calculated. The used transport–reaction equation for the analyte C_A is written as follows (Kockmann, 2008):

$$\frac{\partial C_A}{\partial t} + \nabla \cdot \left(\mathbf{u}_L C_A - D_A \nabla C_A\right) - r = 0 \tag{15}$$

After that, the front position $l(t)$ is updated by using the previous front velocity and the calculated timestep:

$$l(t + \Delta t) = l(t) + ||\mathbf{u}_{L(t)}||\Delta t. \tag{16}$$

Velocity magnitude is updated again by using Eq. 2. Finally the FEM solver is called again as it was previously described. This iterative scheme is reproduced until the velocity front reaches the end of the strip, and consequently, velocity is null throughout the whole strip.

4 Results and discussion

4.1 Validation against numerical calculations

First of all, model predictions are compared to numerical simulations of the full transport problem solved by FEM. The amount of complex formed as a function of flow rate is considered. The curves plotted in Fig. 2a were obtained from Eq. 12, for constant KC_A^0 and KC_S^0 (dimensionless analyte and capture sites concentration, respectively) and predefined values of V_S/V_L (reacted sample volume relative to reaction volume). Symbols are the numerical results for the same parameter values, obtained as described in the previous section. A close agreement is observed, notably at intermediate sample volumes. In particular, for very low sample volumes (dotted line in Fig. 2a) the model overestimates the rate of complex formation, which is due to the initial condition used in the derivation of the analytical solution (Eq. 10). In fact, the model implicitly assumes that the immunoreaction starts with the reaction volume completely filled. The numerical calculation instead reflects the real situation: the reaction volume is filled by capillary flow and the reaction proceeds gradually until $V_S(t) = V_L$. Then, for $V_S \geq V_L$, both calculations predict the same complex formation in the full range of relative flow rates considered. On the other hand, the analytical model detaches from numerical results for sample volumes $V_S = 8V_L$ and higher. This behavior is also expected because of the assumption of constant fluid velocity through the test line. In fact, Eq. 6 is valid for assay times equivalent to a few residence times, nt_r, say $n < 10$. According to Eq. 2, the flow rate decreases as the fluid front advances, and $u_L(nt_r) = u_L(t_r)/(1 + nw_L/x_L)$. In Fig. 2a, $x_L = 20$ mm, $w_L = 1$ mm, thus u_L decreases about 30% for $n = 8$. It is worth noting however that real-world lateral flow tests involve effective x_L distances around $3 - 5$ cm, as they include sample and conjugate pads upstream the membrane (Wong and Tse, 2009); therefore the model could predict reasonably well for larger V_S.

Figure 2b presents model predictions obtained with KC_A^0 varying four orders of magnitude, for fixed sample volume an capture site concentration. Finally, Fig. 2c shows the influence of the KC_S^0 on the amount of complex formed, for fixed values of analyte concentration and sample volume. In both cases, lines were obtained from Eq. 12 and symbols are simulation results obtained with the full numerical formulation. A close matching of calculations is observed for wide ranges of U, KC_A^0 , and KC_S^0 (several orders of magnitude), which constitutes a validation of the analytical model against rigorous numerical formulation.

It is worth to remark that computer simulations involve the full transport problem, while Eq. 12 neglects molecular diffusion. The quantitative agreement found in the validation suggests that molec-

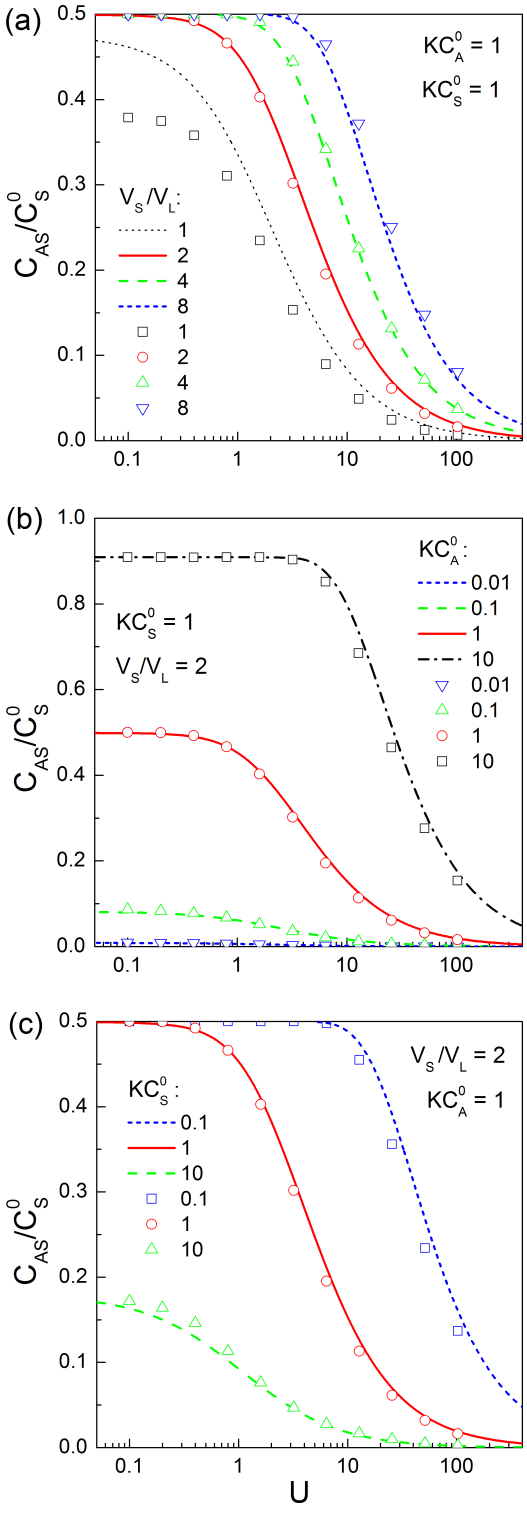

Fig. 2: Relative concentration of complex formed as a function of the relative flow rate. In all cases, lines are the prediction of Eq. 11 and symbols are the results of FEM simulation. 3D numerical data of $C_{AS}(U)$ were converted to 1D by integrating the complex concentration over the whole computational domain. Curves correspond to: **(a)** different values of V_S/V_L for fixed KC_A^0 and KC_S^0 , **(b)** different KC_A^0 for fixed V_S/V_L and KC_S^0, and **(c)** different KC_S^0 for fixed KC_A^0 and V_S/V_L.

ular diffusion is effectively irrelevant in the operating regime of lateral flow assays. The overall shape of curves in Fig. 2 reflects the fact that, for a given sample volume, slow flow rates give more time to molecules to increase the probability of collisions and analyte binding. On the contrary, if the sample flows relatively fast, a fraction of analyte molecules could not bind the capture sites before exiting the reaction zone, and therefore the conversion is poor. The numerical simulation also considers a large flow domain that expands upstream and downstream the test line, with fluid velocity locally varying along the path. The domain of the analytical model is the reaction zone, however the magnitude of fluid velocity is controlled by both the test line location x_L and the membrane coefficient c. Thus one may conclude that the model comprises the key governing factors of lateral flow assays.

In summary, the analytical model can be safely used to attain quantitative predictions for the practical ranges of immunoreaction constant rates, analyte concentrations, capture sites concentrations and typical membranes used in lateral flow test. The only restriction to be taken into account in calculations is that assay times should be higher than t_r (equivalently, $V_S > V_L$) and lower than about 10 t_r (equivalently, $V_S < 10\ V_L$). However, this last constraint can be relaxed for relatively large test line locations (say, $x_L > 20 w_L$).

4.2 Model prediction of time-dependent processes

Here we illustrate model predictions for time evolution of the analyte capture process, while analyzing the interplay between the following operating conditions: fixed sample volume- unlimited assay time, and fixed assay time-unlimited sample volume, as previously discussed by (Parsa et al, 2008) for surface capture in open microchannels. As in lateral flow tests the sample volume is limited, we start with the first situation. The right analysis of the problem comes from Eq. 11, where the reaction dynamics is scaled with the residence time.

Figure 3 shows the prediction of Eq. 11 for different values of U. All the curves are plotted for $KC_A^0 = 1$, so that the maximum sites occupation is 50%. It is worth noting that, for a given residence time, the conversion improves at the lowest flow rates. Of course, assay time and flow rate are inversely proportional, as illustrated in the inset of Fig. 3. For example, if the sample volume to pass by the capture zone is limited to $2V_L$, more than 90% of the attainable equilibrium binding can be attained working at $U = 0.1$. However the assay time will be impractically long. Furthermore, in the limiting case of vanishing fluid velocity the batch process operating regime is virtually reached.

In order to fulfill the analysis, Fig. 4 presents the prediction of Eq. 10, where the analyte capture process is scaled with the kinetic time. It is observed that the conversion for a given time improves with flow rate. This result, in apparent contradiction with the previous one (Fig. 3), is the trend typically expected in the kinetic analysis of advection-diffusion-reaction systems (Gervais and Jensen, 2006; Kockmann, 2008; Hansen et al, 2012; Aguirre et al, 2014). The rationale is that flow rate must be increased to improve the analyte flux, and hence attain better capture efficiency in a given assay time. The drawback of this operation mode is that the sample volume required to attain a given capture

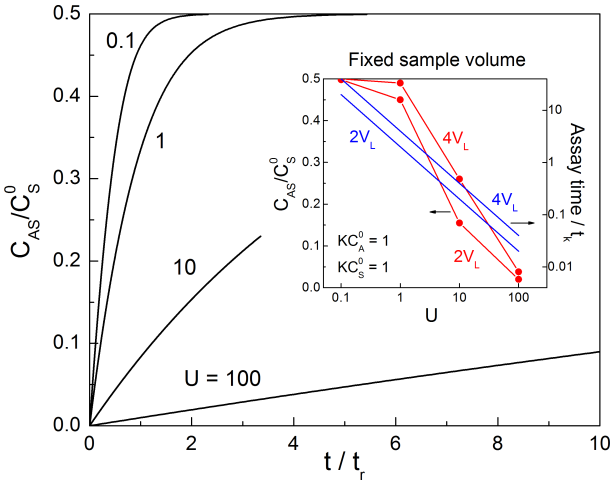

Fig. 3: Relative concentration of complex formed as a function of the relative time (flow scaling). The inset shows both the relative concentration and the assay time required, as a function of the relative fluid velocity, for the specified sample volumes. A sample volume equal to nV_L passes through the reaction zone during an assay time equal to nt_r.

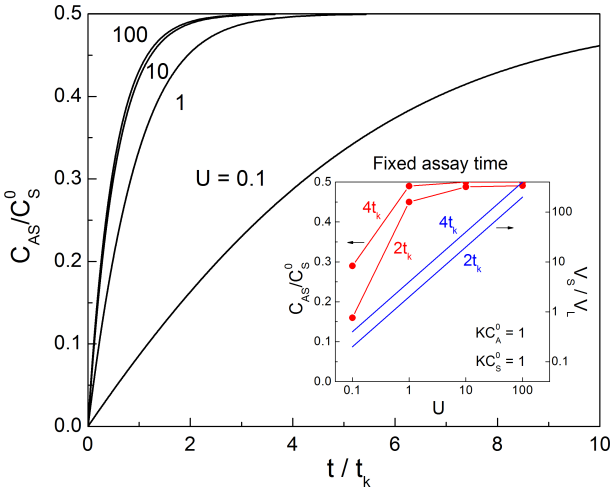

Fig. 4: Relative concentration of complex formed as a function of the relative time (kinetic scaling). The inset shows both the amount of complex formed and the reacted sample volume for the specified reaction times, as a function of the relative fluid velocity.

level increases with flow rate, as shown in the inset of Fig. 4. For example, if one needs to reach 90% of attainable equilibrium binding in a time equivalent to $2t_k$, then the sample volume needed is around 100 times the reaction volume. In other words, increasing the fluid velocity minimizes the assay time, but requires much more sample to pass through the reaction zone to attain the desired capture level. Representations like Fig. 4 are thus misleading for lateral flow tests.

4.3 Practical use of model predictions

Finally we highlight how model predictions are valuable information for the design and development of lateral flow assays. Figure 5 shows the effect of both analyte concentration and sample volume on the amount of complex formed, at each flow rate. It is observed that increasing the fluid velocity for a given analyte concentration (from (a) to (b), full line) produces the same effect on the amount

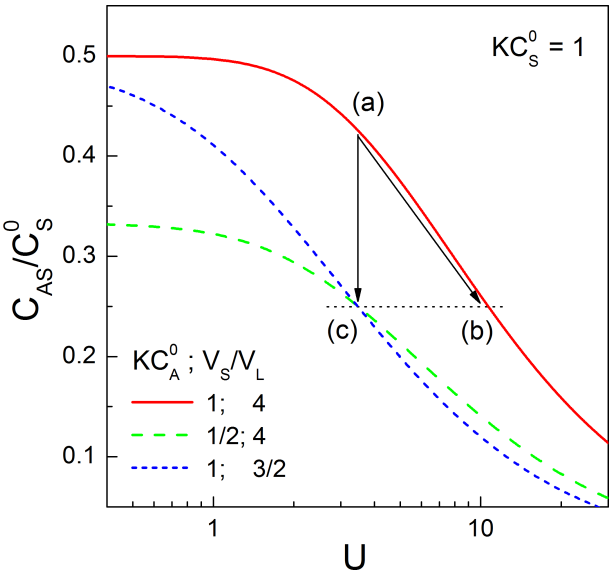

Fig. 5: Relative concentration of complex formed as a function of the relative fluid velocity, for different values of the dimensionless analyte concentration and sample volume. The arrows indicate alternative ways to obtain a different conversion level (dashed line) from an arbitrary situation (a).

of complex formed that keeping the original fluid velocity but decreasing the analyte concentration (from (a) to (c), dashed line). In addition the same effect is obtained by limiting the amount of sample (dotted line) for a given analyte concentration. Of course, the opposite happens by decreasing U or, alternatively, increasing KC_A^0 .

In this sense, it must be noted that there is an empirical rule (widely diffused among test strip developers) saying that the effective concentration of analyte in the sample is inversely proportional to the square of the change in flow rate. The argument is that, when the flow rate doubles, the analyte has half the time to react, and considering a second order reaction, the impact on the amount of complex formed would be equivalent to reduce the analyte concentration by a factor 4. Figure 5 shows that, although the predicted trend is right, the quantitative relation of the aforementioned rule is not necessarily accurate. Furthermore, it is clearly seen that the effective analyte concentration for a given flow rate depends on the considered region of parameters space; hence a single prescription cannot be given for general use. Precisely, the benefits of the model proposed here is that it enables quantitative predictions in terms of the main parameters governing the system, in a wide range of practical conditions.

Finally, Fig. 6 presents an example of diagrams to be studied in the parameter space of the system, namely the dimensionless analyte concentration and the relative fluid velocity. The regions plotted correspond to operation windows defined by the percentage of complex formed. The contour lines were arbitrarily chosen for the purposes of illustration. The diagram in Fig. 6 condense the results discussed above: relatively low flow rates are required to attain better capture efficiencies in samples with low analyte concentrations. Conversely, high flow rates can be implemented in dealing with concentrated samples, which also means shorter assay times. The white region in the bottom of the diagram indicates the practical limit of detection of the system.

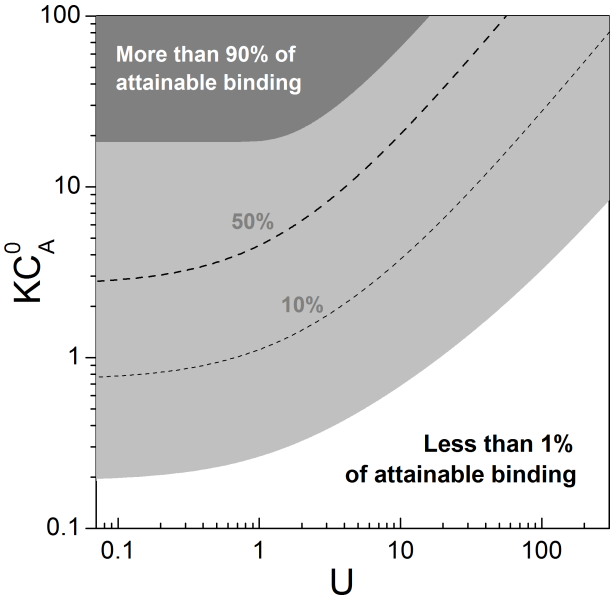

Fig. 6: Parameter space of the system. The different regions are defined by the percentage of complex formed, for a fixed sample volume ($V_S = 4V_L$) and capture sites concentration ($KC_S^0 = 10$).

5 Conclusions

Throughout this work we have described the derivation and practical uses of an analytical model for the dynamics of analyte capture in paper-like membranes, which is the central problem of lateral flow tests. The formulation accounts for the capillary-driven flow through the porous membrane, the advective transport of analyte, and the immunoreactions that takes place in the detection line. The included approximations are physically consistent with the operating regime of lateral flow assays, as probed by the satisfactory comparison of model predictions against full numerical simulations implemented in our lab.

From the fundamental point of view, the proposed model condense the main design parameters of lateral flow assays into two dimensionless numbers: the relative flow rate and the relative analyte concentration. Then the system can be completely characterized in the parameter space of these critical numbers. In addition, the model is able to describe the time evolution of analyte binding by using alternative time scalings. Results are quite interesting, and not necessarily intuitive, as the fraction of bound sites changes significantly depending on the imposed conditions of fixed sample volume or fixed assay time. To our knowledge, the quantitative assessment of lateral flow assays by such a simple, though robust, analytical model has not been reported before in the scientific literature.

From the practical point of view, the equations reported here are valuable tools for the development of strip test. In fact, informed decisions can be made on basic questions such as the appropriate flow rate, sample concentration, or assay time, which in turn are constrained by requirements of sensitivity and detection limits. For example, the model enables a quantitative analysis of the mandatory tradeoff between sample volume and assay time, both of which are to be minimized to fulfill the advantages of microfluidics for point-of- care biosensors.

Acknowledgements The authors acknowledge the financial support from the Consejo Nacional de Investigaciones Científicas y Técnicas, CONICET (PIP-0363), and the Universidad Nacional del Litoral, UNL (CAI+D-78-5012011010010-0).

References

Aguirre A, Kler PA, Berli CL, Collins SE (2014) Design and operational limits of an atr-ftir spectroscopic microreactor for investigating reactions at liquid–solid interface. Chem Eng J 243:197–206

Ayachit U (2015) The paraview guide: A parallel visualization application

Cate DM, Adkins JA, Mettakoonpitak J, Henry CS (2015) Recent developments in paper-based microfluidic devices. Anal Chem 87(1):19–41

Choi JR, Liu Z, Hu J, Tang R, Gong Y, Feng S, Ren H, Wen T, Yang H, Qu Z, et al (2016) Polydimethylsiloxane-paper hybrid lateral flow assay for highly sensitive point-of-care nucleic acid testing. Anal Chem . DOI:10.1021/acs.analchem.6b0195

Donea J, Huerta A (2003) Finite Element Methods for Flow Problems. Wiley Online Library

Elizalde E, Urteaga R, Berli CL (2015) Rational design of capillary-driven flows for paper-based microfluidics. Lab Chip 15(10):2173–2180

Gervais T, Jensen KF (2006) Mass transport and surface reactions in microfluidic systems. Chem Eng Sci 61(4):1102–1121

Hansen R, Bruus H, Callisen TH, Hassager O (2012) Transient convection, diffusion, and adsorption in surface-based biosensors. Langmuir 28(19):7557–7563

Hu G, Gao Y, Sherman PM, Li D (2005) A microfluidic chip for heterogeneous immunoassay using electrokinetical control. Microfluid Nanofluid 1(4):346–355

Jahanshahi-Anbuhi S, Chavan P, Sicard C, Leung V, Hossain SZ, Pelton R, Brennan JD, Filipe CD (2012) Creating fast flow channels in paper fluidic devices to control timing of sequential reactions. Lab Chip 12(23):5079–5085

Kler PA, Berli CL, Guarnieri FA (2011) Modeling and high performance simulation of electrophoretic techniques in microfluidic chips. Microfluid Nanofluid 10(1):187–198

Kler PA, Dalcin LD, Paz RR, Tezduyar TE (2013) Supg and discontinuity-capturing methods for coupled fluid mechanics and electrochemical transport problems. Comput Mech 51(2):171–185

Kockmann N (2008) Transport phenomena in micro process engineering. Springer Science & Business Media, Berlin

Mace CR, Deraney RN (2014) Manufacturing prototypes for paper-based diagnostic devices. Microfluid Nanofluid 16(5):801–809

Masoodi R, Pillai KM (2010) Darcy's law-based model for wicking in paper-like swelling porous media. AIChE J 56(9):2257–2267

Mendez S, Fenton EM, Gallegos GR, Petsev DN, Sibbett SS, Stone HA, Zhang Y, López GP (2009) Imbibition in porous membranes of complex shape: quasi-stationary flow in thin rectangular seg-

ments. Langmuir 26(2):1380–1385

Moghadam BY, Connelly KT, Posner JD (2015) Two orders of magnitude improvement in detection limit of lateral flow assays using isotachophoresis. Anal Chem 87(2):1009–1017

Parolo C, Medina-Sánchez M, de la Escosura-Muñiz A, Merkoçi A (2013) Simple paper architecture modifications lead to enhanced sensitivity in nanoparticle based lateral flow immunoassays. Lab Chip 13(3):386–390

Parsa H, Chin CD, Mongkolwisetwara P, Lee BW, Wang JJ, Sia SK (2008) Effect of volume-and time-based constraints on capture of analytes in microfluidic heterogeneous immunoassays. Lab Chip 8(12):2062–2070

Qian S, Bau HH (2003) A mathematical model of lateral flow bioreactions applied to sandwich assays. Anal Biochem 322(1):89–98

Qian S, Bau HH (2004) Analysis of lateral flow biodetectors: competitive format. Anal Biochem 326(2):211–224

Ragavendar M, Anmol CM (2012) A mathematical model to predict the optimal test line location and sample volume for lateral flow immunoassays. In: Engineering in Medicine and Biology Society (EMBC), IEEE, pp 2408–2411

Shin JH, Park J, Kim SH, Park JK (2014) Programmed sample delivery on a pressurized paper. Biomicrofluidics 8(5):054,121

Shou D, Fan J (2015) Structural optimization of porous media for fast and controlled capillary flows. Phys Rev E 91(5):053,021–6

Squires TM, Messinger RJ, Manalis SR (2008) Making it stick: convection, reaction and diffusion in surface-based biosensors. Nat Biotechnol 26(4):417–426

van der Walt S, Colbert S, Varoquaux G (2011) The numpy array: A structure for efficient numerical computation. Comput Sci Eng 13(1):22–30

Wang X, Hagen JA, Papautsky I (2013) Paper pump for passive and programmable transport. Biomicrofluidics 7(1):014,107–11

Wong R, Tse H (eds) (2009) Lateral Flow Immunoassay. Humana Press, New York

Yager P, Edwards T, Fu E, Helton K, Nelson K, Tam MR, Weigl BH (2006) Microfluidic diagnostic technologies for global public health. Nature 442(7101):412–418

Yetisen AK, Akram MS, Lowe CR (2013) Paper-based microfluidic point-of-care diagnostic devices. Lab Chip 13(12):2210–2251

Zeng N, Wang Z, Li Y, Du M, Liu X (2012) Identification of nonlinear lateral flow immunoassay state-space models via particle filter approach. IEEE Trans Nanotech 11(2):321–327